ACS APPLIED ENERGY MATERIALS

www.acsaem.org Letter

Examining Effects of Negative to Positive Capacity Ratio in Three-Electrode Lithium-Ion Cells with Layered Oxide Cathode and Si Anode

Mei Luo, Marco-Tulio F. Rodrigues, Leon L. Shaw, and Daniel P. Abraham*

Cite This: ACS Appl. Energy Mater. 2022, 5, 5513−5518 Read Online

ACCESS | Metrics & More | Article Recommendations | Supporting Information

ABSTRACT: The negative to positive electrode capacity ratio (*n*:*p*) is crucial for lithium-ion cell design because it affects both energy density and long-term performance. In this study, the effect of the *n*:*p* ratio on electrochemical performance has been investigated for NMC532/Si cells containing a reference electrode. By monitoring individual electrode potentials, depths of lithiation/delithiation at the anode and cathode could be determined. The superior performance of the higher *n*:*p* cell, including greater reversibility, better capacity retention, and lower impedance rise, can be attributed to smaller volume changes in the silicon particles during electrochemical cycling.

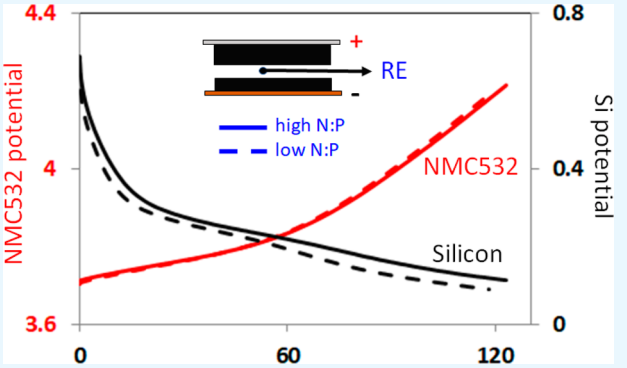

KEYWORDS: *n:p ratio, reference electrode, Si-dominant anode, NMC532 cathode, electrode impedance*

INTRODUCTION

Lithium-ion batteries (LIBs) have revolutionized portable electronics in recent decades and are poised to play a big role in the transportation sector, with major automakers announcing a transition to electric vehicles.[1,2] As this field advances rapidly, much effort has been spent on developing novel materials to break through the energy and power density limits of LIBs. Silicon, as the most promising next-generation anode candidate, has been widely studied because of its high specific capacity, but large volume changes during cycling produces stress on particles, causing pulverization and electrical isolation of silicon domains.[3−5] Moreover, stability of the solid electrolyte interphase (SEI) is disrupted by the dimensional changes, causing additional Li^+ ions to be trapped and leading to capacity decay. Many strategies, such as new material architectures[6−8] and electrode formulations,[9−11] have been suggested for improving the electrochemical behavior of the silicon anode by addressing its intrinsic challenges; however, studies are often conducted in cells with a lithium counter electrode, causing certain conclusions and claims to be overstated.[12,13]

Investigation of the silicon anode in full-cells is necessary for practical applications because cell performance over time is affected by the limited lithium inventory and the interplay between the cathode and anode properties. An often overlooked topic is cell capacity balancing, i.e., the areal capacity ratio of the negative and positive electrodes (*n*:*p* ratio), which is crucial for the safety and cycle life of practical LIBs.[14−16] Here, an important consideration is lithium plating, as the deposited Li can react with the surrounding electrolyte to form products that immobilize Li^+ ions.[14,17−19] To mitigate this risk, a slight oversizing of negative electrode capacity is used in practical applications. Naturally, this surplus anode weight requires a sacrifice in specific energy,[20,21] so the trade-off between energy and safety must be considered during cell design.

Capacity balancing is especially critical for cells with Si-bearing anodes, as these can be designed such that the silicon particles are utilized to a lesser extent, thereby decreasing volume changes during cycling. Accurately identifying terminal electrode potentials is difficult for silicon anodes because of their sloped voltage profiles.[14,15] Information on these voltage profiles can be obtained in three-electrode cells, which contain a reference electrode in addition to the positive and negative electrodes. In this Letter, we present data obtained on three-electrode cells and examine the effect of varying *n*:*p* ratios on cell capacity, capacity retention, and impedance and on the changes in electrode potentials during cycling. The cells contain a $LiNi_{0.5}Mn_{0.3}Co_{0.2}O_2$ (NMC532) cathode, a Si-

Received: March 3, 2022
Accepted: April 27, 2022
Published: May 2, 2022

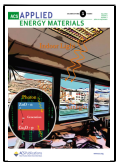

Table 1. Charge/Discharge Capacities Used to Determine *n*:*p* Ratios for the Two NMC/Si Cells

		system 1			system 2	
full-cell	charge	discharge	CE %[a]	charge	discharge	CE %
mAh/cm^2	1.86	1.30	70.1	1.80	1.25	69.5
Si half-cell	lithiation	delithiation	CE %	lithiation	delithiation	CE %
mAh/cm^2	2.64	2.39	90.5	2.17	1.89	87.1
n:*p* ratio		1.83			1.51	

[a]CE = Coulombic efficiency, %.

dominant anode, and a Li-metal microprobe reference electrode to monitor cathode and anode potentials; see experimental details in the Supporting Information (SI). We obtained *n*:*p* ratios of 1.51 and 1.83 by adjusting mass loading of the silicon anode while keeping the same cathode. Additional figures are included in the SI to complement data shown in this text; these figures are designated by S, for example, Figure S1. This study provides insights on how to design full-cells with silicon anodes to achieve longer lifetimes.

RESULTS AND DISCUSSION

Following the convention proposed in our previous study,[22] we calculated the *n*:*p* ratios as being the first delithiation areal capacity of the silicon half-cell (in the 0.01−1.5 V cycling range) divided by the discharge areal capacity of the first cycle of each full-cell. As shown in Table 1 and Figure S1, the *n*:*p* ratios of the NMC//Si cells were 1.51 and 1.83. Despite employing Si anodes with loadings varying by 26%, both cells exhibited similar initial Coulombic efficiencies; this happens because of the interplay between various factors in the cell. For example, in the thicker electrode, the increase in surface area is counterbalanced by a lower Si expansion and higher cathode utilization, decreasing the initial capacity losses. In fact, the cell with a higher *n*:*p* ratio exhibited a higher initial discharge capacity.

Three-electrode cells can monitor the real-time evolution of electrode potentials (Figure 1a), providing unique information to explain cell behavior. The voltage profiles for both electrodes during the third formation cycle (C/20 rate) are shown in Figure 1b. At the end of charge (EOC), a higher *n*:*p* ratio causes both cathode and anode ending potentials to be higher, indicating differences in electrode utilization. With higher *n*:*p* ratios, more Li^+ is extracted from the cathode, but a smaller fraction of the total anode capacity is utilized, i.e., the degree of lithiation/delithiation of the electrodes is different for different *n*:*p* ratios.

Cycling data for NMC/Si cells with different *n*:*p* ratios are compared in Figure 2, with high and low *n*:*p* ratios indicated by blue and magenta symbols, respectively. The electrode potential profiles at cycles 1, 2, and 100 (all at C/20 rate) are given in Figure S2. The specific capacities with respect to weight of oxide in the cathode are shown in Figure 2a. Although initial capacities are similar, the rate of fade is visibly faster for the cell with a lower *n*:*p* ratio. At the beginning of the C/3 cycles, discharge capacity of the lower *n*:*p* cell is slightly higher than that of the higher *n*:*p* cell. This transient superior capacity, which lasts about 5 cycles, is probably due to the lower polarization and better rate capability of the initially thinner Si anode. At the end of the test, specific capacities are ∼55 and ∼78 mAh/g for cells with an *n*:*p* ratio of 1.51 and 1.83, respectively. The capacity loss at cycle 100 relative to that of cycle 2 is ∼39% for the higher *n*:*p* cell compared with the ∼52% loss for the lower *n*:*p* cell. Coulombic efficiencies were

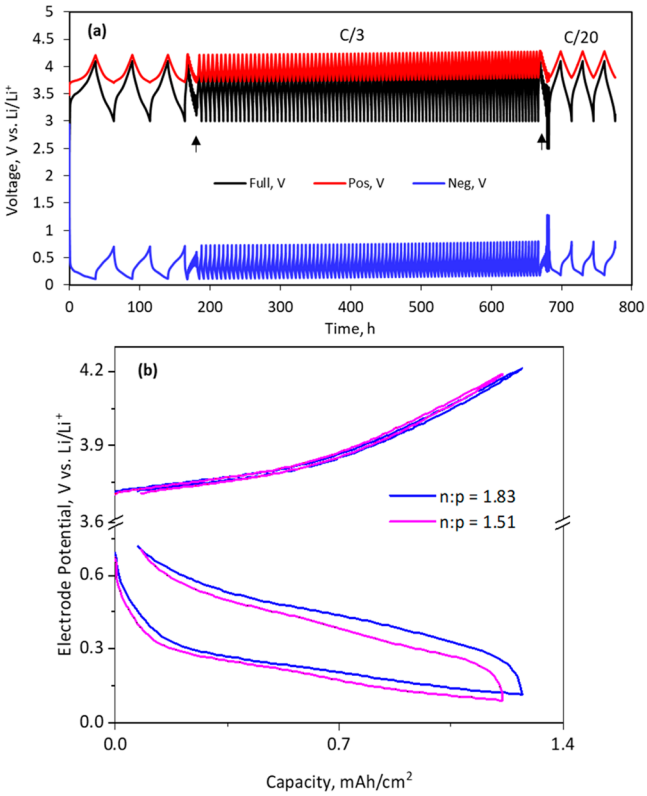

Figure 1. (a) Full-cell voltage, positive electrode potential, and negative electrode potential vs time. Location of HPPC pulses is marked by arrows. (b) Positive electrode potential and negative electrode potential profiles for the 3rd cycle from cells with *n*:*p* = 1.83 (blue profiles) and *n*:*p* = 1.51 (magenta profiles) when the full-cell is cycled between 3 and 4.1 V.

consistently higher for the higher *n*:*p* ratio (Figure 2b), in agreement with the improved capacity retention. Figure 2c shows the capacities normalized by the combined weight of Si and carbon in the anodes, as both materials are electrochemically active. During the formation cycles, the capacities are higher in the cell with a lower *n*:*p* ratio by ∼200 mAh/g_{Si+C}, illustrating the higher utilization of anode capacity. However, the cell capacities also decrease faster; at cycle 100, the accessible anode capacities of the higher and lower *n*:*p* cells are 833 and 731 mAh/g_{Si+C}, respectively (also see Figure S2).

The *anode* potentials at the end of charge (EOC, at 4.1 V) and end of discharge (EOD, at 3 V) for all cycles are shown in Figure 2d. At the beginning of the test, anodes experience potentials as low as 87 mV vs Li/Li^+ at a lower *n*:*p* ratio, but only 109 mV vs Li/Li^+ at a higher *n*:*p* ratio. The final anode lithiation potential increases steadily during the test, at a similar pace for both systems. This is not what would be expected on the basis of Figure 2c: as anode-normalized capacities converge, one would expect electrode potentials to

https://doi.org/10.1021/acsaem.2c00665
ACS Appl. Energy Mater. 2022, 5, 5513−5518

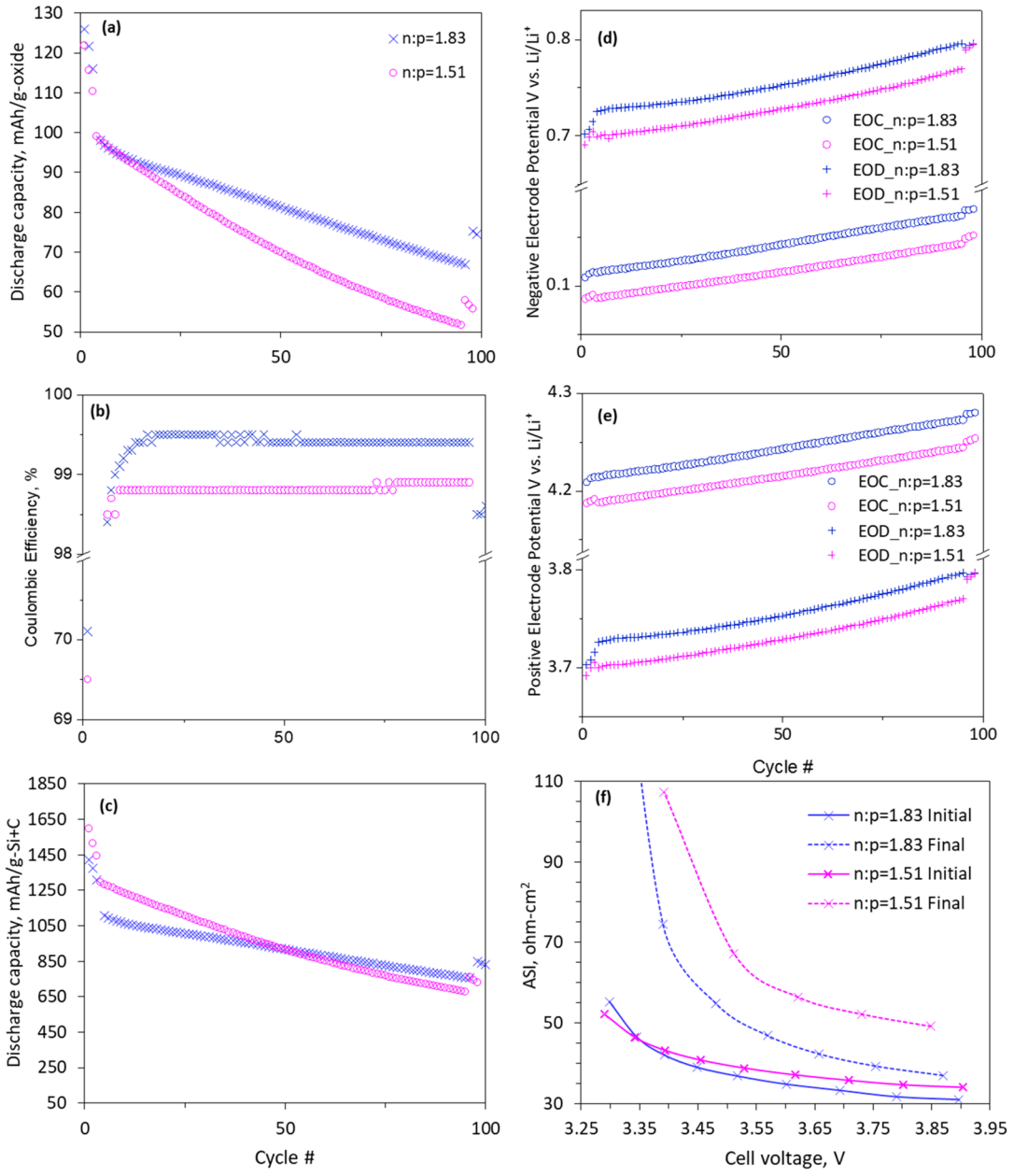

Figure 2. Full-cell data from cells with $n{:}p$ = 1.83 (blue plots) and $n{:}p$ = 1.51 (magenta plots). (a) Specific capacity based on mass of oxide cathode. (b) Coulombic efficiency vs cycle number. (c) Specific capacity based on mass of (Si + C). (d) negative electrode potential and (e) positive electrode potential at the end of charge (EOC) and discharge (EOD). (f) Cell ASI at cycle 4 (initial) and cycle 96 (final), obtained at the locations marked by the arrows in Figure 1a.

also approach similar values. This apparent contradiction can be resolved by considering that Si electrodes can experience a severe loss of accessible capacity during cycling, as Si domains become isolated due to cycling-induced particle fracturing.[3,4] Due to higher utilization of the anode at lower $n{:}p$ ratios, particles are expected to undergo larger levels of expansion, facilitating mechanical damage that leads to permanent capacity loss. Combining the information from Figure 2c,d, it can be concluded that lower $n{:}p$ ratios lead to more prominent isolation of Si domains, causing the smaller amount of incoming Li^+ to suffice to achieve high levels of anode utilization. In other words, faster aging decreases the number of active sites available at the anode, causing low anode potentials to be achieved even at decreasing capacities. This $n{:}p$ ratio dependent Si capacity loss is in agreement with observations from tests with harvested electrodes made in our previous study.[22] Here, the use of a reference electrode makes this information available without the need for post-test experiments.

The EOC and EOD potentials for the cathode are shown in Figure 2e. The higher cutoff potentials observed for the anode at higher $n{:}p$ ratios cause the potentials for the cathode to be proportionally larger. Clearly, both charge and discharge cutoffs are larger by ~26 mV for the cell with $n{:}p$ ratio equal to 1.83. In principle, this could accelerate an impedance rise at the cathode, caused by oxygen loss at the particle surface and/or electrolyte oxidation.[23] To investigate whether this logic applies to cells with Si-dominant electrodes, area-specific impedances (ASIs) were measured and are shown as a function of full-cell voltage in Figure 2f. Unexpectedly, although the

https://doi.org/10.1021/acsaem.2c00665
ACS Appl. Energy Mater. 2022, 5, 5513−5518

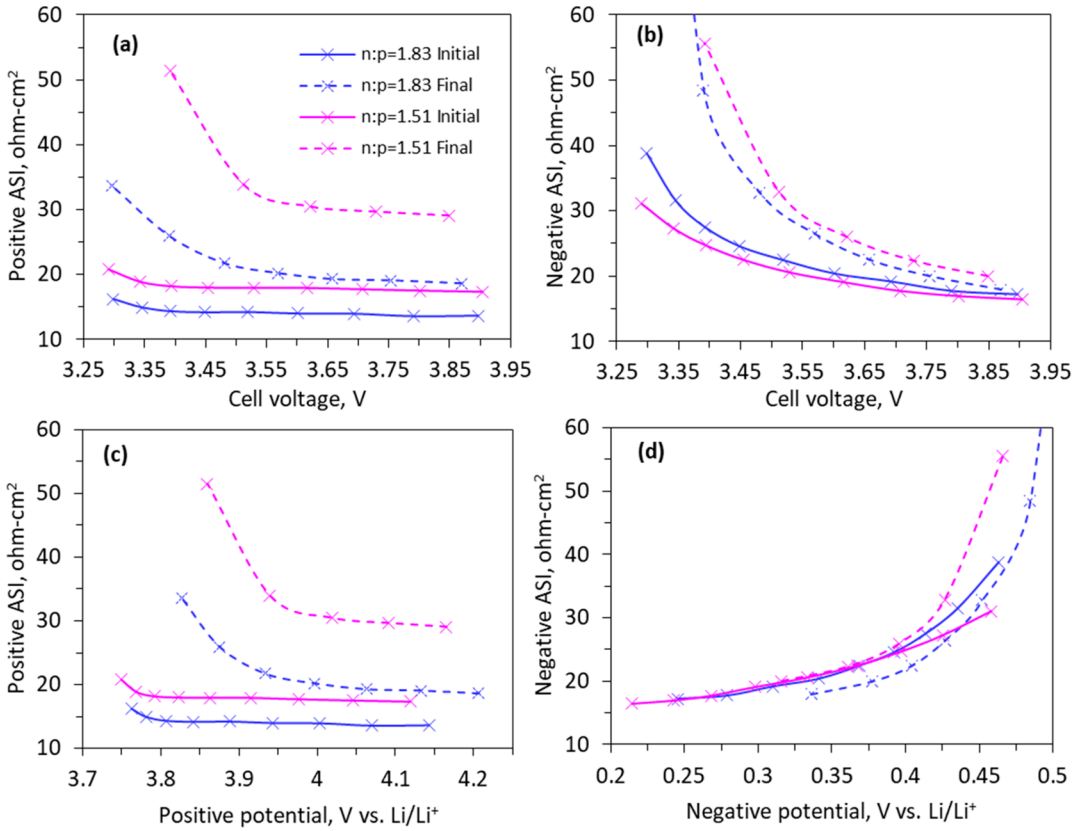

Figure 3. Area-specific impedance (ASI) of (a) positive electrode and (b) negative electrode as a function of full-cell voltage, (c) positive ASI as a function of positive electrode potential, and (d) negative ASI as a function of negative electrode potential for the cells with *n*:*p* = 1.83 (blue profiles) and *n*:*p* = 1.51 (magenta profiles). The ASI values at cycle 4 and cycle 96 (see Figure 1) are termed initial and final, respectively.

initial ASI was similar for both systems, the impedance rise during testing was observed to be *higher* for the cell with lower *n*:*p* ratio.

The use of a three-electrode cell helps decouple the contributions of each electrode to the overall impedance rise observed in the full-cell. Figure 3a,b shows the positive and negative electrode impedances, respectively, as a function of full-cell voltage. The *n*:*p* ratio had little effect on the anode behavior, which consistently exhibited an impedance rise below 3.7 V. Markedly different results are seen for the cathode; despite the lower cathode potentials throughout the test (Figure 2e), the impedance rise was higher for the lower *n*:*p* ratio cell (Figure 3a). To investigate further, we present the electrode ASIs plotted as a function of their respective potentials in Figure 3c,d. Interestingly, the increase in anode impedance reported in Figure 3b is caused by shifts of the electrode potential (slippage) as the full-cell ages (see Figure S3). When the ASI data are plotted as a function of *electrode* potential, it is seen that the anode impedance remains relatively constant (Figure 3d). For the cathode, however, the impedance rise at lower *n*:*p* ratios remains visible in Figure 3c.

What is the origin of this higher cathode impedance rise? It is difficult to postulate a mechanism operating directly at the cathode/electrolyte interface, which can produce a higher impedance rise at lower electrode potentials. One possibility is that processes at the anode can affect the aging behavior of the cathode, i.e., cross talk is taking place.[23,24] We previously proposed that cracking of Si particles allows HF-mediated acidolysis to occur on the freshly exposed surfaces, which can cause partial dissolution of Si-containing species.[25] Some of these species have been observed to deposit and oxidize at the cathode, forming SiO_2-like deposits.[25] The higher utilization of the anode capacity at lower *n*:*p* ratios (Figure 2d), and the consequent higher levels of anode deterioration, suggests that particle cracking/dissolution would be more prevalent in this system, which could make the transport of Si species to the cathode more likely. Although this mechanism could explain the observation of a higher impedance rise at lower cathode potentials (at lower *n*:*p* ratios), a direct link between the formation of SiO_2-like regions at the cathode and an increase in impedance remains to be demonstrated. Nevertheless, our observations suggest that this conjecture merits future investigation.

CONCLUSIONS

This study utilized three-electrode cells to investigate the effect of *n*:*p* ratio (1.83 and 1.51) on electrochemical performance of cells with an NMC532 cathode and 70 wt % Si anode. The cycling results showed that full-cells with a larger *n*:*p* ratio exhibit an improved capacity retention, a higher Coulombic efficiency, and a lower capacity fade. Measurements of electrode potentials indicated that increasing the *n*:*p* ratio limited utilization of the anode and, thus, the volume expansion of the Si particles during lithiation, justifying the improved levels of cell and electrode capacity retention.

Using a reference electrode also allowed us to track individual electrode impedances as the cell aged. When impedances were analyzed as a function of same electrode potential, the *n*:*p* ratio had negligible effects on anode

https://doi.org/10.1021/acsaem.2c00665
ACS Appl. Energy Mater. 2022, 5, 5513−5518

impedance. For the cathode, the impedance trends were unexpected, as the cathode exposed to lower maximum potentials (in cells with lower *n*:*p* ratio) exhibited a much larger impedance rise. We hypothesize that processes at the anode are ultimately responsible for this unexpected behavior. At a lower *n*:*p* ratio, utilization of the anode increases, which also increases the dilation of Si particles during lithiation. These greater volumetric changes would increase fracturing of Si particles, making them more susceptible to acidolysis and dissolution into the electrolyte; subsequent migration and deposition of Si-bearing species at the cathode could increase impedance. This connection between the crossover of anode species and cathode impedance rise is interesting and will be evaluated in future work.

■ ASSOCIATED CONTENT

Supporting Information

The Supporting Information is available free of charge at https://pubs.acs.org/doi/10.1021/acsaem.2c00665.

Experimental details detailing materials and cell assembly and electrochemical characterization, voltage vs capacity profiles used to calculate the *n*:*p* ratios, positive and negative electrode potential profiles for select cycles, and positive and negative electrode potential profiles as hysteresis plots (PDF)

■ AUTHOR INFORMATION

Corresponding Author

Daniel P. Abraham − *Chemical Sciences and Engineering Division, Argonne National Laboratory, Argonne, Illinois 60439, United States;* orcid.org/0000-0003-0402-9620; Email: abraham@anl.gov

Authors

Mei Luo − *Chemical Sciences and Engineering Division, Argonne National Laboratory, Argonne, Illinois 60439, United States; Department of Mechanical, Materials and Aerospace Engineering, Illinois Institute of Technology, Chicago, Illinois 60616, United States;* orcid.org/0000-0002-0548-0707

Marco-Tulio F. Rodrigues − *Chemical Sciences and Engineering Division, Argonne National Laboratory, Argonne, Illinois 60439, United States;* orcid.org/0000-0003-0833-6556

Leon L. Shaw − *Department of Mechanical, Materials and Aerospace Engineering, Illinois Institute of Technology, Chicago, Illinois 60616, United States;* orcid.org/0000-0002-2170-1573

Complete contact information is available at: https://pubs.acs.org/10.1021/acsaem.2c00665

Notes

The submitted manuscript has been created by UChicago Argonne, LLC, Operator of Argonne National Laboratory ("Argonne"). Argonne, a U.S. Department of Energy Office of Science laboratory, is operated under Contract No. DE-AC02-06CH11357. The U.S. Government retains for itself, and others acting on its behalf, a paid-up nonexclusive, irrevocable worldwide license in said article to reproduce, prepare derivative works, distribute copies to the public, and perform publicly and display publicly, by or on behalf of the Government.

The authors declare no competing financial interest.

■ ACKNOWLEDGMENTS

M.L. and L.L.S. acknowledge support from the National Science Foundation INTERNship program. D.P.A. and M.-T.F.R. are grateful for support from DOE's Vehicle Technologies Office (VTO). The electrodes used in this article are from Argonne's Cell Analysis, Modeling and Prototyping (CAMP) Facility, which is fully supported by the VTO. We are grateful to our many colleagues, especially Stephen Trask and Andrew Jansen at Argonne.

■ REFERENCES

(1) Ding, Y.; Cano, Z. P.; Yu, A.; Lu, J.; Chen, Z. Automotive Li-Ion Batteries: Current Status and Future Perspectives. *Electrochem. Energy Rev.* **2019**, *2* (1), 1−28.

(2) Bresser, D.; Hosoi, K.; Howell, D.; Li, H.; Zeisel, H.; Amine, K.; Passerini, S. Perspectives of Automotive Battery R&D in China, Germany, Japan, and the USA. *J. Power Sources* **2018**, *382*, 176−178.

(3) Casimir, A.; Zhang, H.; Ogoke, O.; Amine, J. C.; Lu, J.; Wu, G. Silicon-Based Anodes for Lithium-Ion Batteries: Effectiveness of Materials Synthesis and Electrode Preparation. *Nano Energy* **2016**, *27*, 359−376.

(4) Wetjen, M.; Solchenbach, S.; Pritzl, D.; Hou, J.; Tileli, V.; Gasteiger, H. A. Morphological Changes of Silicon Nanoparticles and the Influence of Cutoff Potentials in Silicon-Graphite Electrodes. *J. Electrochem. Soc.* **2018**, *165* (7), A1503−A1514.

(5) Yu, D. Y. W.; Zhao, M.; Hoster, H. E. Suppressing Vertical Displacement of Lithiated Silicon Particles in High Volumetric Capacity Battery Electrodes. *ChemElectroChem.* **2015**, *2* (8), 1090−1095.

(6) He, Q.; Ashuri, M.; Liu, Y.; Liu, B.; Shaw, L. Silicon Microreactor as a Fast Charge, Long Cycle Life Anode with High Initial Coulombic Efficiency Synthesized via a Scalable Method. *ACS Appl. Energy Mater.* **2021**, *4* (5), 4744−4757.

(7) Xie, J.; Tong, L.; Su, L.; Xu, Y.; Wang, L.; Wang, Y. Core-Shell Yolk-Shell Si@C@Void@C Nanohybrids as Advanced Lithium Ion Battery Anodes with Good Electronic Conductivity and Corrosion Resistance. *J. Power Sources* **2017**, *342*, 529−536.

(8) Chan, C. K.; Peng, H.; Liu, G.; McIlwrath, K.; Zhang, X. F.; Huggins, R. A.; Cui, Y. High-Performance Lithium Battery Anodes Using Silicon Nanowires. *Nat. Nanotechnol.* **2008**, *3* (1), 31−35.

(9) Shen, X.; Tian, Z.; Fan, R.; Shao, L.; Zhang, D.; Cao, G.; Kou, L.; Bai, Y. Research Progress on Silicon/Carbon Composite Anode Materials for Lithium-Ion Battery. *Journal of Energy Chemistry* **2018**, 1067−1090, DOI: 10.1016/j.jechem.2017.12.012.

(10) Yao, K. P. C.; Okasinski, J. S.; Kalaga, K.; Almer, J. D.; Abraham, D. P. Operando Quantification of (De)Lithiation Behavior of Silicon−Graphite Blended Electrodes for Lithium-Ion Batteries. *Adv. Energy Mater.* **2019**, *9* (8), 1803380.

(11) Li, Q.; Liu, X.; Han, X.; Xiang, Y.; Zhong, G.; Wang, J.; Zheng, B.; Zhou, J.; Yang, Y. Identification of the Solid Electrolyte Interface on the Si/C Composite Anode with FEC as the Additive. *ACS Appl. Mater. Interfaces* **2019**, *11* (15), 14066−14075.

(12) Li, H. Practical Evaluation of Li-Ion Batteries. *Joule* **2019**, *3* (4), 911−914.

(13) Chae, S.; Ko, M.; Kim, K.; Ahn, K.; Cho, J. Confronting Issues of the Practical Implementation of Si Anode in High-Energy Lithium-Ion Batteries. *Joule* **2017**, *1* (1), 47−60.

(14) Kasnatscheew, J.; Placke, T.; Streipert, B.; Rothermel, S.; Wagner, R.; Meister, P.; Laskovic, I. C.; Winter, M. A Tutorial into Practical Capacity and Mass Balancing of Lithium Ion Batteries. *J. Electrochem. Soc.* **2017**, *164* (12), A2479−A2486.

(15) Obrovac, M. N.; Chevrier, V. L. Alloy Negative Electrodes for Li-Ion Batteries. *Chem. Rev.* **2014**, *114* (23), 11444−11502.

(16) Reuter, F.; Baasner, A.; Pampel, J.; Piwko, M.; Dörfler, S.; Althues, H.; Kaskel, S. Importance of Capacity Balancing on The

Electrochemical Performance of Li[Ni $_{0.8}$ Co $_{0.1}$ Mn $_{0.1}$]O $_2$ (NCM811)/Silicon Full Cells. *J. Electrochem. Soc.* **2019**, *166* (14), A3265−A3271.
(17) Waldmann, T.; Hogg, B. I.; Wohlfahrt-Mehrens, M. Li Plating as Unwanted Side Reaction in Commercial Li-Ion Cells − A Review. *J. Power Sources* **2018**, *384*, 107−124.
(18) Legrand, N.; Knosp, B.; Desprez, P.; Lapicque, F.; Raël, S. Physical Characterization of the Charging Process of a Li-Ion Battery and Prediction of Li Plating by Electrochemical Modelling. *J. Power Sources* **2014**, *245*, 208−216.
(19) Liu, Q.; Du, C.; Shen, B.; Zuo, P.; Cheng, X.; Ma, Y.; Yin, G.; Gao, Y. Understanding Undesirable Anode Lithium Plating Issues in Lithium-Ion Batteries. *RSC Adv.* **2016**, *6* (91), 88683−88700.
(20) Son, B.; Ryou, M. H.; Choi, J.; Kim, S. H.; Ko, J. M.; Lee, Y. M. Effect of Cathode/Anode Area Ratio on Electrochemical Performance of Lithium-Ion Batteries. *J. Power Sources* **2013**, *243*, 641−647.
(21) Abe, Y.; Kumagai, S. Effect of Negative/Positive Capacity Ratio on the Rate and Cycling Performances of LiFePO4/Graphite Lithium-Ion Batteries. *J. Energy Storage* **2018**, *19*, 96−102.
(22) Rodrigues, M. T. F.; Prado, A. Y. R.; Trask, S. E.; Ahmed, S.; Jansen, A. N.; Abraham, D. P. Modulating Electrode Utilization in Lithium-Ion Cells with Silicon-Bearing Anodes. *J. Power Sources* **2020**, *477*, 229029.
(23) Rodrigues, M.-T. F.; Kalaga, K.; Trask, S. E.; Shkrob, I. A.; Abraham, D. P. Anode-Dependent Impedance Rise in Layered-Oxide Cathodes of Lithium-Ion Cells. *J. Electrochem. Soc.* **2018**, *165* (9), A1697−A1705.
(24) Xiong, D. J.; Petibon, R.; Nie, M.; Ma, L.; Xia, J.; Dahn, J. R. Interactions between Positive and Negative Electrodes in Li-Ion Cells Operated at High Temperature and High Voltage. *J. Electrochem. Soc.* **2016**, *163* (3), A546−A551.
(25) Bareño, J.; Shkrob, I. A.; Gilbert, J. A.; Klett, M.; Abraham, D. P. Capacity Fade and Its Mitigation in Li-Ion Cells with Silicon-Graphite Electrodes. *J. Phys. Chem. C* **2017**, *121* (38), 20640−20649.

https://doi.org/10.1021/acsaem.2c00665
ACS Appl. Energy Mater. 2022, 5, 5513−5518